Journal Name

Communication

Polymeric Acid-doped Transparent Carbon Nanotube Electrodes in Organic Solar Cells with the Longest Doping Durability

Received 00th January 20xx,
Accepted 00th January 20xx

DOI: 10.1039/x0xx00000x

www.rsc.org/

Il Jeon,[a‡] Clement Delacou,[a‡] Hiroshi Okada,[a] Graham E. Morse,[b] Tae-Hee Han,[c] Yuta Sato,[d] Anton Anisimov,[e] Kazu Suenaga,[a,d] Esko I. Kauppinen,[f] Shigeo Maruyama,*[a,g] Yutaka Matsuo*[a,h]

This communication reports the discovery of the polymeric acid, tetrafluoroethylene-based fluoropolymer-copolymer sulfonic acid, functioning as an effective *p*-type dopant for transparent carbon electrodes. The polymeric acid exhibits high doping effectiveness which is durable for more than one year. Carbon nanotube transparent electrodes doped by the polymeric acid were used in organic solar cells. The devices show excellent efficiency with remarkable stability owing to the polymeric acid's strong acidity and stability.

Transparent electrodes are vital components for touch panels, displays, and photovoltaic cells. Widely used indium tin oxide (ITO) transparent electrodes are not suitable for flexible electronics because of their brittleness, high cost, and diffusion of impurities within the devices.[1,2] Carbon electrodes, such as carbon nanotube (CNT)[3–5] and graphene electrodes[6–9], have recently shown considerable promise as ITO replacement, but they fall short of conductivity.[10] To offset this weakness, dopants must be used to increase the conductivity of the carbon electrode by increasing the concentration of their free carriers and reduce resistance.[11] A myriad of carbon electrode dopants have been reported to date. In particular, HNO_3, MoO_3, and $AuCl_3$ have been widely used as *p*-type chemical dopants. For an ideal transparent electrode dopant, certain requirements must meet: conductivity, doping durability, transparency, morphology, and handling safety. Many of the conventional dopants have limitations in these regards. For example, the HNO_3 has low durability in ambient due to its volatile property, causing a rapid decrease in electrical conductivity over a short period of time.[12,13] The use of $AuCl_3$ results in formation of 50–100 nm Au particles that inhibit charge flow, increasing current leakage, and thereby lowering the device efficiency.[14] MoO_3 is a durable dopant, but it requires thermal evaporation and annealing at approximately 300°C to induce a significant doping effect.[15] As reported by Lee and colleagues, trifluoromethanesulfonic acid (TFMS) displayed nearly ideal durability when used to dope graphene in organic light emitting diodes.[16] TFMS nonetheless does not exhibit permanent durability and has an issue with handling safety due to its high volatility and corrosive nature.

Recognizing this, we investigated the use of high molecular weight polymeric dopant (sulfonated tetrafluoroethylene-based fluoropolymer-copolymer sulfonic acid i.e., Nafion®) in transparent conductive CNT films. The sulfonic acid has been reported to dope carbon electrodes effectively without damaging the framework of the carbon network.[17] We expected that entanglement of the CNT network and the long chains of the polymeric acid would provide an exceptionally durable doping effect without increasing the defects in the carbon species. In this communication, the polymeric acid was compared with the two established acidic dopants, HNO_3 and TFMS, using various techniques. This study showed that the polymeric acid possessed similar doping effectiveness but superior durability in comparison with the other dopants. The excellent durability came from the low volatility and high stability of the conjugate base of the acid, as demonstrated by the analyses. Its doping durability is nearly permanent, because it has been more than one year as of the submission of this manuscript, yet the doping effect is still intact. In addition, due to its high molecular weight, the polymeric acid is substantially safer to handle than the other volatile acids.[18,19] Moreover, the application of the polymeric acid on CNT improved the

[a] *Department of Mechanical Engineering, The University of Tokyo, 7-3-1 Hongo, Bunkyo-ku, Tokyo 113-8656, Japan.*
[b] *Chilworth Technical Centre, Merck Chemicals Ltd., University Parkway, SO16 7QD Southampton, UK.*
[c] *Department of Materials Science and Engineering, University of California, Los Angeles, Los Angeles, CA 90095, USA*
[d] *Nanomaterials Research Institute, National Institute of Advanced Industrial Science and Technology, Tsukuba 305-8565, Japan.*
[e] *Canatu Ltd., Konalankuja 5, FI-00390 Helsinki, Finland.*
[f] *Department of Applied Physics, Aalto University School of Science, FI-00076 Aalto, Finland.*
[g] *Research Institute for Energy Conservation, National Institute of Advanced Industrial Science and Technology, Tsukuba 305-8565, Japan.*
[h] *Hefei National Laboratory for Physical Sciences at the Microscale, University of Science and Technology of China, 96 Jinzhai Road, Hefei, Anhui 230026, China.*
Electronic Supplementary Information (ESI) available: [details of any supplementary information available should be included here]. See DOI: 10.1039/x0xx00000x

morphology, which is critical to the device performance when used as the transparent electrode. The polymeric acid-doped CNT films satisfied the key requirements for a transparent carbon electrode, which are the high optical transparency, high conductivity, permanent doping durability, good morphology, and safety of handling. To test their device applicability, organic solar cells (OSCs) were fabricated using a newly developed PBTZT-stat-BDTT-8 polymer as the photoactive system. To test the durability of the polymeric acid-doped CNT films as the transparent bottom electrode, the OSCs have to be stable to make a valid evaluation. PBTZT-stat-BDTT-8 system is known to be one of the most stable OSCs reported thus far.[20,21] The OSCs using the polymeric acid-doped CNT electrode produced a PCE of 8.0% initially, which was almost retained for more than 60 days, while the ITO-based OSCs with an initial PCE of 9.1% dropped to below 8.0%, because of suspected degradation of ITO by poly(3,4-ethylenedioxythiophene)-poly(styrenesulfonate) (PEDOT:PSS) and metal ion diffusion. The devices using the polymeric acid dopant were much more durable than the devices using the other dopants on account of its remarkable doping durability.

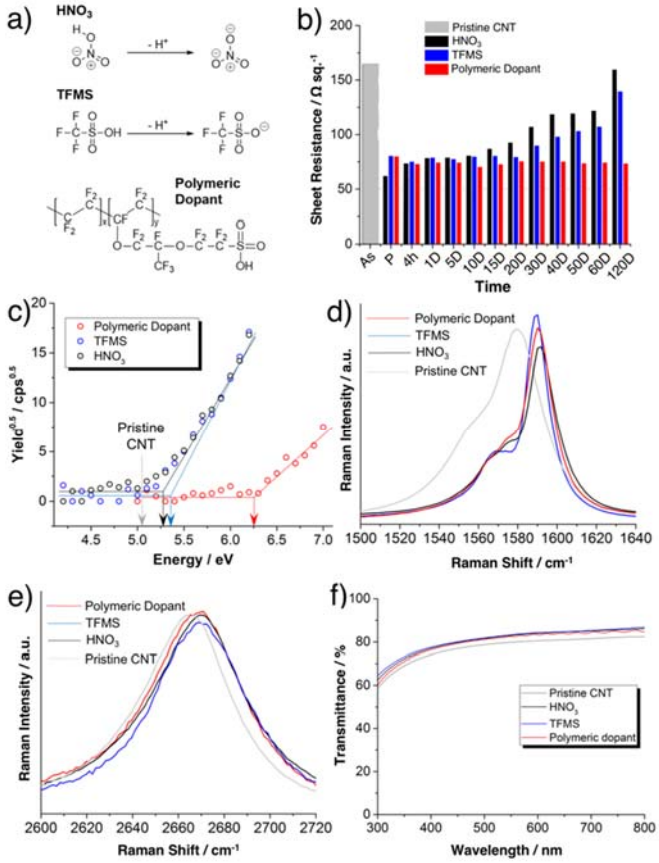

Fig. 1. a) Three acids compared in this work. b) Bar graph showing the four-probe sheet resistance stability data of the three types of doped CNT films and the pristine CNT film over 4 months in air (25 °C, 50% relative humidity). c) PYS spectra of the three types of doped CNT films and the pristine CNT film. Raman shifts of the d) G bands and e) 2D bands of the three types of doped CNT films and the pristine CNT film. f) Transmittance data of the three types of doped CNT films and the pristine CNT film.

Solution-processed *p*-type HNO_3-, TFMS-, and polymeric acid-doped CNT films were compared on their doping effectiveness and durability (**Fig. 1a**). The sheet resistance of the films was measured by the four-probe measurement over a long period of storage in air (25 °C, 50% relative humidity) (**Fig. 1b**). Upon doping, the average sheet resistance of the CNT films (80% transmittance at 550 nm) decreased to more than half, from about 170 Ω $sq.^{-1}$ to *ca.* 75 Ω $sq.^{-1}$. The HNO_3-doped CNT films initially showed slightly lower sheet resistance (*ca.* 60 Ω $sq.^{-1}$) than that of the TFMS- and the polymeric acid-applied CNT films, but the resistance of the HNO_3-doped CNT films increased back within 4 h. The doping effect of both TFMS and the polymeric acid lasted much longer; although the resistance of the TFMS-doped CNT films started to increase after 1 month, the polymeric acid-doped CNT films persisted for more than 4 months. As of this writing (more than one year after the initial measurement) the doping effect of the polymeric acid still remains intact. Photoelectron yield spectroscopy (PYS) was used to analyze changes in the Fermi level after doping (**Fig. 1c**). The PYS data show that both HNO_3 and TFMS doping decreased the Fermi level of the CNT films by approximately 0.3 eV, confirming successful doping. In the case of polymeric acid doping, the Fermi level decreased greatly by *ca.* 1.2 eV to -6.3 eV. We conjecture that such dramatic decrease was due to the large amount of fluorinated chain on the polymeric acid[23] rather than a stronger doping effect. As the PYS data did not give a concrete result, we conducted Raman spectroscopy. It shows the *p*-type doping effect in the form of upshifted G and 2D bands arising from the phonon stiffening effect.[24–27] From Fig. 1d and e, we can see that both the G and 2D bands of the doped CNT samples exhibited marked shifts to higher binding energy. However, the differences between the three dopants were marginal. We can conclude that the strengths of the initial doping effect in CNT films were similar among these three dopants which concurs with the four probe measurement in Fig. 1b. Transmittance is a critical factor for the transparent conductive electrodes. Therefore, a UV-vis transmittance measurement was carried out on the different acid-doped CNT films. The data showed that all of the doped CNT films had similar transmittance, indicating that all of those acids, especially the polymeric acid, qualify for a dopant for transparent electrodes (**Fig. 1f**). The small increase in the overall transmittance, despite the increase in charge carrier density, is suspected to be due to dissolution of CNT catalysts upon acid doping.[28]

We applied the three acidic dopants to a different type of carbon electrodes, graphene, and studied the doping effect and durability (**Fig. S1**) In the reflection of the CNT data, the doping effect and durability were weaker for graphene. This could be because of the larger surface area and entangled geometry of CNTs. The doping effect and durability in graphene followed the trend reported by T.-H. Han *et al.,*[16] which shows that the doping effect of TFMS was much stronger than that of HNO_3. However, the doping effects of HNO_3 and TFMS were equally strong for CNT electrode. We speculate that this is due to the solvent being trapped inside the network of CNTs which may not dry as well as the solvents on graphene. For the polymeric acid doping, both CNT and graphene electrodes displayed similarly strong doping effect and excellent durability.

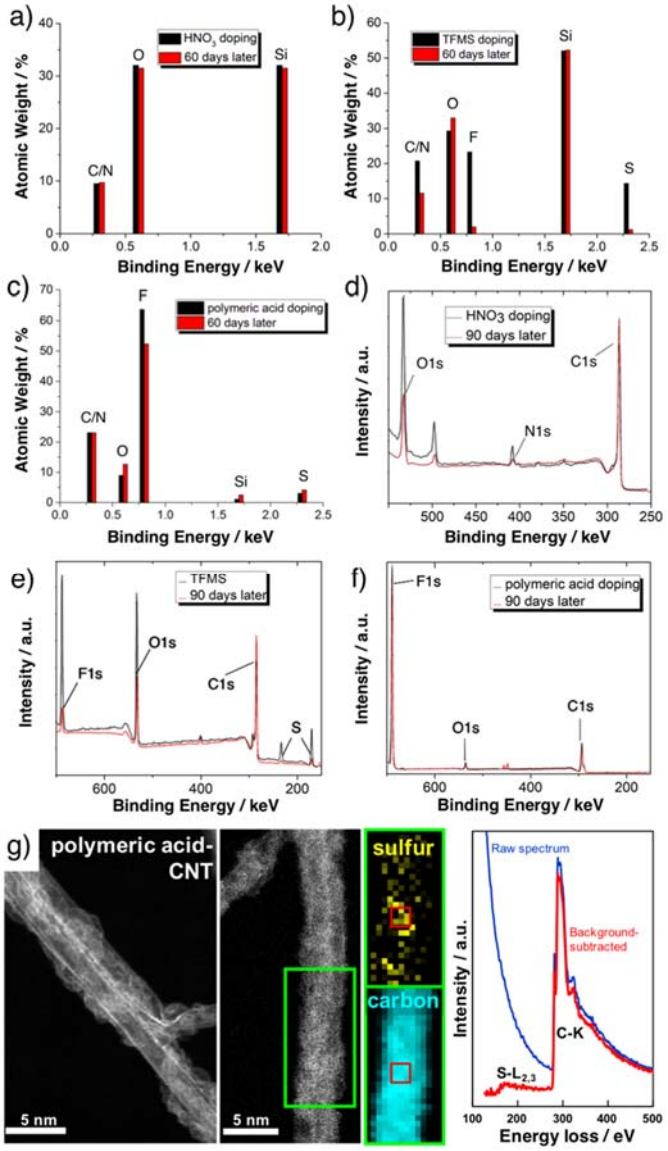

Fig. 2. EDX elemental analyses of a) HNO_3-doped CNT films, b) TFMS-doped CNT films, and c) polymeric acid-doped CNT films soon after doping and 60 days later. XPS spectra of d) HNO_3-doped CNT films, e) TFMS-doped CNT films, and f) polymeric acid-doped CNT films soon after doping and 90 days later. g) STEM image of 90 days old polymeric acid-doped CNT film in which, the polymeric acids are wrapped around a CNT strand according to the EELS chemical mapping analysis.

The doping mechanism can be viewed from either protonation or reduction potential points of view. Regardless of the details of the doping mechanism, it is indisputable that the stability and volatility of the acid and its conjugate base have a direct impact on the durability of the doping.[3] Therefore, the stability and volatility of the acid and its conjugate base next to CNT electrode were investigated using scanning electron microscopy (SEM) together with energy dispersive X-ray analysis (EDX), and X-ray photoelectron spectroscopy (XPS) (**Fig. 2 and S2; Table S1**). In the case of the elemental analysis by SEM EDX, HNO_3-doped CNT did not show the relative abundance of HNO_3 or NO_3^-, because the energy levels of N and C being too close (**Fig. 2a**). In the case of the TFMS- and polymeric acid-doped CNT films, it was clear that the amount of TFMS significantly decreased after 60 days, as indicated by the substantial decreases in the F and S peaks (**Fig. 2b**). On the other hand, the F and S peaks of the polymeric dopant remained almost unchanged (**Fig. 2c**). XPS provides much more accurate measurements with higher resolution, though the measurement had to be done on a small area. The XPS data shows a clear decrease in the N peak after 90 days this time for HNO_3, providing evidence that the disappearance of HNO_3/NO_3^- was directly linked to the short doping durability of HNO_3 (**Fig. 2d**). TFMS/triflate ions also decreased after 90 days, revealing its limited durability, though they lasted longer than HNO_3 (**Fig. 2e**). The polymeric dopant/conjugate base again remained almost unchanged (**Fig. 2f**), though the S peak was difficult to observe due to low intensity. These results denote that the durability of the doping effect is directly related to the volatility of the acid. Further analysis using scanning transmission electron microscopy (STEM) enables physical observation of TFMS disappearing from CNT while the polymeric acid remains unchanged after 90 days (**Fig. S3**). Electron energy loss spectroscopy (EELS) chemical mapping analysis shows that sulfur atoms from the polymeric acid are wrapping around the carbons of CNT strand from the TEM image (**Fig. 2g**).[29–32] We can deduce that the fluorinated polymer chains in the polymeric acid can protect CNTs from oxidation and contamination, prolonging the doping effect even further.[33,34]

Morphology of the transparent electrodes plays a crucial role for the device performance in any type of solar cells. Atomic force microscopy (AFM) images and the roughness mean squared (RMS) values in **Fig. S4** show the polymeric acid-doped CNT has much smoother surface compared with the bare CNT, and HNO_3- and TFMS-doped CNT films (**Fig. S1**). The fact that the polymeric acid can smoothen the intrinsically rough CNT electrode surface is a remarkable advantage over the other acidic dopants.[5,7,28] The cross-sectional scanning electron microscopic (SEM) images show that 2%-diluted Nafion solution thoroughly seep through the network of CNTs (**Fig. S5**). Wettability of the transparent electrode is also an important factor in solar cell fabrication. According to the water contact angle test, applying HNO_3 and TFMS to CNTs reduced the surface energy of CNTs greatly, enabling the direct PEDOT:PSS coating on top (**Fig. S6**). However, applying the polymeric acid to CNTs did not decrease the surface energy of CNTs as much, leaving it still hydrophobic. This meant that the spin-coating of hydrophilic PEDOT:PSS was not possible, and we had to either modify PEDOT:PSS by adding a surfactant (0.5 wt% polyoxyethylene(6) tridecyl ether) to make PEDOT:PSS hydrophobic, or deposit a thin layer of MoO_3 (2nm) before spin-coating PEDOT:PSS.[28,35-36]

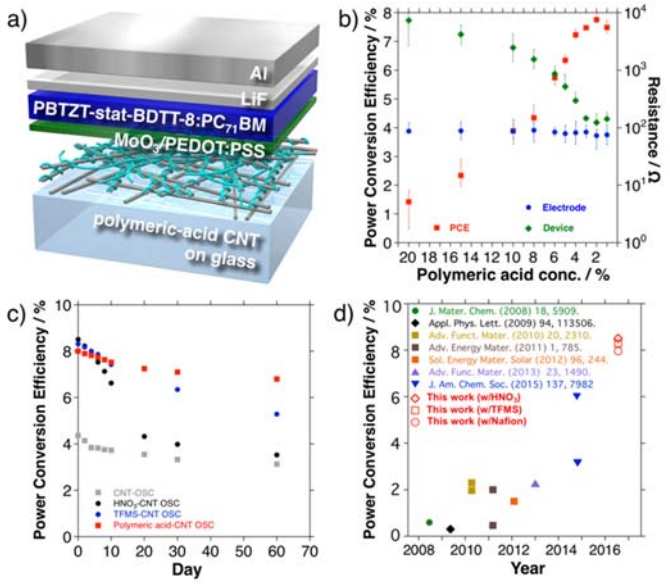

Fig. 3. a) Schematics of the polymeric acid-doped CNT film-based OSC used in this work. b) Graph representing average power conversion efficiencies of OSCs with ranges (red square) for the y_1-axis on the left, and averages and ranges of polymeric acid-doped CNT electrode resistance (blue circle) and device resistance (green diamond) values for the y_2-axis on the right, according to the concentration of applied polymeric acid solution. c) Stability test data of OSCs kept over 60 days under dark in N_2 condition d) Reported PCEs of indium-free CNT-based OSCs.

The doping durability of CNT transparent electrodes in OSCs was tested using a mixture of PBTZT-stat-BDTT-8 and $PC_{71}BM$ as the photo-active layer (**Fig. 3a**). This is because PBTZT-stat-BDTT-8-based OSCs have demonstrated excellent air-stability and performance.[20,21] Using stable OSC for this test is crucial for monitoring the doping durability, because the degradation of the organic active layer can be misinterpreted as the weakening of the doping effect. MoO_3/PEDOT:PSS was used as the charge selective layer, because OSCs with surfactant-added PEDOT:PSS produced a slightly lower performance and surfactant-added PEDOT:PSS-based OSCs cannot be used on HNO_3-CNT and TFMS-CNT electrodes (**Table S2**). OSCs with ITO, CNT, HNO_3-CNT, TFMS-CNT, and polymeric acid-CNT were fabricated and compared. **Table 1** shows the initial PCEs and the photovoltaic parameters of the OSCs (**Fig. S7**). Compared with the pristine CNT-based OSCs, the polymeric acid-doped CNT-based OSCs demonstrated a substantial increase in PCE, owing to strong doping effect. However, the devices gave a slightly lower PCE (8.0%) than those of the other dopants-used devices (8.5% for HNO_3-CNT OSCs and 8.3% of TFMS-CNT OSCs) (**Table 1**). The lower PCE came from the higher series resistance (R_S). The polymeric acid, Nafion® is known to be a proton conductor, which means it requires water molecules to conduct holes through the Grotthuss mechanism. The internal resistance of the polymer backbones must have caused the marginal drop in fill factor (FF). According to **Fig. 3b**, it can be seen that the PCE of the device increases with the decrease in the concentration of the Nafion solution.[37,38] The device resistance values obtained by dividing R_S by the active area follows the efficiency trend, indicating that diluting the Nafion solution produced a thinner polymeric acid film on the CNT electrodes. The resistance of the polymeric acid doped-CNT was not dependent on the dilution concentration when measured by the two probe measurement using an ohmmeter; the sheet resistance of the polymeric acid-doped CNT films measured by the four-probe measurement also produced the same trend. Despite the slightly lower initial PCE, the polymeric acid-doped CNT OSCs retained the PCE for 60 days, ending up with the highest PCE of 7.01% among the tested devices (**Fig. 3c, Table 1**). During the stability test, the devices were stored inside a glove box (N_2) in the dark. In contrast to encapsulation of devices, this protected the devices from the degradation of both the active material and metal electrode while allowing dopants to leave the device system at their will.[39] It should be mentioned that the ITO-based devices and HNO_3-CNT-based devices degraded rather quickly over time. We suspect that such degradation of the ITO-based devices is due to ITO being etched by the acidic PEDOT:PSS, which leads to metal ion migration (**Table 1, Fig. S8**).[13,40,41] The PCEs obtained in this work are currently the highest efficiencies reported among the indium-free CNT-based OSC devices (**Fig. 3d**). The performance is by far efficient and stable compared with the second best devices with a PCE of 6.04%, which was reported by our group using thieno[3,4-b] thiophene/benzodithiophene (PTB7) and MoO_x.[4]

Table 1. Photovoltaic parameters of the OSCs using different dopants-doped CNT films as the electrode under one sun illumination (AM 1.5 G, 100 mW cm^{-2}) with initial PCEs and PCEs measured 60 days later. All the values are given in two significant figures. The statistical analysis is given in Table S3.

Electrode	J_{SC} (mA cm^{-2})	V_{OC} (V)	FF	R_S (Ω cm^2) [60 days later]	R_{SH} (Ω cm^2)	PCE (%) [60 days later]
ITO	15.0	0.81	0.75	4.3 [21]	1200	9.1 [7.0]
CNT	12.0	0.80	0.46	60 [78]	320	4.4 [3.1]
HNO_3-CNT	14.2	0.81	0.74	9.0 [64]	1100	8.5 [3.5]
TFMS-CNT	14.1	0.81	0.73	10 [34]	1100	8.3 [5.3]
polymeric acid-CNT	14.3	0.80	0.70	16 [21]	1200	8.0 [7.0]

Conclusions

we demonstrated that this polymeric sulfonic acid is an effective dopant with excellent durability for more than one year in both CNT and graphene electrodes. The doping effectiveness of the polymeric acid was on par with that of the established dopants, HNO_3 and TFMS, while the durability of the polymeric acid was far superior. Such exceptional stability stemmed from its high molecular weight and long fluorinated chains, which formed an entangled network with the CNTs, as evidenced by various analyses including STEM. The fluorinated conjugate base with heavy molecular weight stabilized donated protons while protecting them from oxygen and water. The doped CNT films were used in OSC devices and showed high efficiency. Although the polymeric acid showed slightly lower performance initially, its remarkable doping durability led to the highest maintained PCE after 60 days compared to the control devices. This efficiency is the record PCE among the reported indium-free CNT-based OSC devices.

Experimental section

Carbon Nanotube Film Synthesis. Single-walled CNTs were synthesized by an aerosol (floating catalyst) CVD method based on ferrocene vapor decomposition in a CO atmosphere. The catalyst precursor was vaporized by passing room temperature CO through a cartridge filled with ferrocene powder. The flow containing ferrocene vapor was then introduced into the high-temperature zone of a ceramic tube reactor through a water-cooled probe and mixed with additional CO. To obtain stable growth of single-walled CNTs, a controlled amount of CO_2 was mixed with the CO carbon source. single-walled CNTs were directly collected downstream of the reactor by filtering the flow through a nitrocellulose or silver membrane filter (Millipore Corp., USA; HAWP, 0.45 μm pore diameter).

Graphene Film Synthesis. Continuous films of graphene were synthesized by means of alcohol-catalytic chemical vapor deposition (ACCVD) on copper using ethanol as the carbon source. Commercial copper foil (Nilaco Corp., CU-113303) was successively sonicated in HCl, DI-water, and IPA for 10 minutes each. The cleaned foil was then left to oxidize on a hot plate at 250°C for 1 hour. After oxidation, the foil was crimped in the shape of a pocket enclosure and loaded into the quartz tube of a home-made CVD reaction chamber that was evacuated to 15 Pa. The reaction chamber was heated to the target temperature of 1065°C under a constant flow rate of 300 sccm of 3% H_2 diluted in Argon throughout the reaction. A butterfly valve was used to maintain the total pressure within the quartz tube at 300 Pa for the duration of the growth procedure. After reaching the target temperature of 1065°C, the copper foil was left to anneal for one additional hour under constant flow of Ar/H_2. After the annealing process was completed, a constant flow of 0.1 sccm of ethanol vapor was introduced to initiate growth. Growth times (as measured from start of the introduction of the ethanol vapor) varied between 4 and 10 hours, with longer growth times leading to larger graphene single crystals. It took 8-10 hours of growth to yield fused regions of graphene single crystals, leading to a continuous, conductive film of graphene. Upon completion of the growth step, the furnace was turned off and the quartz tube bearing the graphene-impregnated copper films was cooled using a fan for 30 minutes under the flow of 300 sccm Ar gas to prevent the collapse of the copper pockets. Immediately after synthesis and cooling, the pocket was opened and subjected to a contrasting oxidation on a hotplate at 250°C for 1 minute to discern the regions of the copper films with graphene (which did not oxidize) from those without graphene, which developed a colorful film of copper oxide. The regions bearing continuous graphene film were then transferring using the wet-etching poly(methyl methacrylate) (PMMA) transfer process explained extensively in previous works.

Dopant Preparation. Dopants concentrations were optimized in the way that the CNT films used in this work demonstrate the maximum doping effects.

Nitric Acid (HNO_3). A 5 μL droplet of 35% concentrated HNO_3 (Wako) was applied to the center of the 1 × 1 cm^2 carbon electrodes to avoid contact with indium at four corners and dried at 80 ℃ for 10 min.

Trifluoromethanesulfonic Acid (TFMS). TFMS solution was prepared by diluting 2% of TFMS (>98% purity, from TCI) in nitromethane. 20 μL of this solution was applied to the carbon electrodes and spin-coated at 5000 rpm for 60 s preceded by a 30 s acceleration step. The samples were then dried at 100 ℃ for 1 h.

Polymeric Acid (Nafion). 20 wt. % of Nafion® perfluorinated resin solution in a mixture of lower aliphatic alcohols and water was spin-coated on the carbon electrodes at 7000 rpm for 60 s preceded by a 30 s acceleration step. The samples were then dried at 100 ℃ for 1 h.

Characterizations. Four probe was measured by a home-built system. Shimadzu UV-3150 was used for the UV-vis measurement. The Fermi levels were measured by Riken Keiki PYS in air (AC-2). They were calibrated by Au before the measurement. The samples for the PYS measurements were prepared on glass substrates by spin-coating the solutions at an rpm of 3000 for 30 s inside a glove box. The samples were kept in N_2, but exposed to air and light before the PYS measurement. These films were thermally annealed at 100℃ for 5 min. Both homemade systems based on Seki Technotron STR-250 (excitation wavelength 532 nm) and inVia Raman microscope (Renishaw) were used for the Raman measurement. Core level photoemission measurements were performed by XPS (PerkinElmer, 5400MC) using monochromatic Al Kα radiation. The XPS resolution was estimated to be ≈1 eV and the energy offset was calibrated using the surface C 1s peak. SEM analysis of the CNT film was performed using an S-4800 (Hitachi). EDX was performed using EDX/SEM TM3030Plus (Hirachi High-Technologies Corporation). STEM images of CNT electrodes were obtained using a JEOL JEM-2100F electron microscope equipped with double JEOL Delta spherical aberration correctors at a reduced electron accelerating voltage of 60 kV to minimize irradiation-induced damage. EELS measurement was carried out using a Gatan Quantum electron spectrometer attached to the microscope. Elemental distributions of carbon

and sulfur were determined by the intensities of their K and L edges, respectively, at each measured point in the scanned areas for STEM-EELS chemical mapping. J–V characteristics were measured by software-controlled source meter (Keithley 2400) in dark conditions and 1 sun AM 1.5G simulated sunlight irradiation (100 mW/cm^2) using a solar simulator (EMS-35AAA, Ushio Spax Inc.) with Ushio Xe short ark lamp 500, which was calibrated using a silicon diode (BS-520BK, Bunkokeiki).

Device Fabrication. Patterned ITO substrates (15 × 15 mm) with a sheet resistance of 9 Ω sq^{-1} (Techno Print Co., Ltd.) were used. The substrates were sonicated sequentially in cleaning surfactant (Semi Clean, M-Lo), water, acetone and 2-isopropanol for 15 min each. The ITO substrates were exposed to UV/O_3 for 15 min. A PEDOT:PSS dispersion in water (CleviosPVP, Heraeus Precious Metals GmbH & Co.) was spin-coated on either ITO or a thermally deposited 2-nm-thick MoO_3 film at 4500 rpm for 45 s. This was followed by the deposition of PBTZT-stat-BDTT-8 photoactive layer mixed with [6]-phenyl C71-butyric acid methyl ester ($PC_{71}BM$) in 1:3 ratio at a concentration 60 mg ml^{-1} in ortho-dichlorobenzene (anhydrous, 99%, Sigma Aldrich Chemical Co., Inc.). The active solution was spin-coated onto target substrates at 1000 rpm for 30 s without a filter. LiF and Al were thermally deposited with thicknesses of 1 nm and 100 nm, respectively.

Conflicts of interest

There are no conflicts to declare

Notes and references

‡These authors contributed equally.

Acknowledgements

I.J. thanks the Research and Education Consortium for Innovation of Advanced Integrated Science by Japan Science and Technology (JST). This work was supported by Japan Society for the Promotion of Science (JSPS) KAKENHI Grant Numbers JP25107002, JP15H05760, JP16H04187, JP17K19116, JP17H06609, JP16K05948, JP16H06333 and IRENA Project by JST-EC DG RTD, Strategic International Collaborative Research Program, SICORP. Part of this work is based on results obtained from a project commissioned by the New Energy and Industrial Technology Development Organization (NEDO). This work was partly supported by the MOPPI project of the Aalto University AEF research program.

1 H. Kim, J. Byun, S.-H. Bae, T. Ahmed, J.-X. Zhu, S.-J. Kwon, Y. Lee, S.-Y. Min, C. Wolf, H.-K. Seo, J.-H. Ahn and T.-W Lee, *Adv. Energy Mater.*, 2016, **6**, 1600172.
2 S.-H. Bae, H. Zhao, Y.-T. Hsieh, L. Zuo, N. D. Marco, Y. S. Rim, G. Li and Y. Yang, *Chem.*, 2016, **1**, 197–219.
3 L. Yu, C. Shearer and J. Shapter, *Chem. Rev.*, 2016, **116**, 13413–13453.
4 I. Jeon, K. Cui, T. Chiba, A. Anisimov, A. G. Nasibulin, E. I. Kauppinen, S. Maruyama and Y. Matsuo, *J. Am. Chem. Soc.*, 2015, **137**, 7982–7985.
5 I. Jeon, T. Chiba, C. Delacou, Y. Guo, A. Kaskela, O. Reynaud, E. I. Kauppinen, S. Maruyama and Y. Matsuo, *Nano Lett.*, 2015, **15**, 6665–6671.
6 T.-H. Han, M.-H. Park, S.-J. Kwon, S. H. Bae, H.-K. Seo, H. Cho, J.-H. Ahn and T.-W. Lee, *NPG Asia Mater.*, 2016, **8**, e303.
7 I. Jeon, J. Yoon, N. Ahn, M. Atwa, C. Delacou, A. Anisimov, E. I. Kauppinen, M. Choi, S. Maruyama and Y. Matsuo, *J. Phys. Chem. Lett.*, 2017, **8**, 5395–5401.
8 H. Kim, S.-H Bae, T.-H. Han, K.-G. Lim, J.-H. Ahn and T.-W. Lee, *Nanotechnology.*, 2014, **25**, 014012.
9 H. Kinoshita, I. Jeon, M. Maruyama, K. Kawahara, Y. Terao, D. Ding, R. Matsumoto, Y. Matsuo, S. Okada and H. Ago, H., *Adv. Mater.*, 2017, **29,** 1702141.
10 J. Du, S. Pei, L. Ma and H.-M. Cheng, *Adv. Mater.*, 2014, **26,** 1958–1991.
11 U. N. Maiti, W. J. Lee, J. M. Lee, Y. Oh, J. Y. Kim, J. E. Kim, J. Shim, T. H. Han, and S. O. Kim, *Adv. Mater.*, 2014, **26**, 40–67.
12 F. Güneş, H.-J. Shin, C. Biswas, G.H. Han, E. S. Kim, S. J. Chae, J.-Y. Choi, and Y. H. Lee, *ACS Nano*, 2010, **4**, 4595–4600.
13 T.-H. Han, Y. Lee, M.-R. Choi, S.-H. Woo, S.-H. Bae, B. H. Hong, J.-H. Ahn and T.-W. Lee, *Nat. Photonics*, 2012, **6**, 105–110.
14 S. M. Kim, K. K. Kim, Y. W. Jo, M. H. Park, S. J. Chae, D. L. Duong, C. W. Yang, J. Kong and Y. H. Lee, *ACS Nano*, 2011, **5**, 1236–1242.
15 S. L. Hellstrom, M. Vosgueritchian, R. M. Stoltenberg, I. Irfan, M. Hammock, Y. B. Wang, C. Jia, X. Guo, Y. Gao and Z. Bao, *Nano Lett.*, 2012, **12**, 3574–3580.
16 T.-H. Han, S.-J Kwon, N. Li, H.-K. Seo, W. Xu, K. S. Kim and T.-W. Lee, *Angew. Chemie Int. Ed.*, 2016, **55**, 6197–6201.
17 Y.-R. Shin, I.-Y. Jeon and J.-B. Baek, *Carbon*, 2012, **50**, 1465–1476.
18 Y. Kim, J. Ryu, M. Park, E. S. Kim, J. M. Yoo, J. Park, J. H. Kang and B. H. Hong, *ACS Nano*, 2014, **8**, 868–874.
19 I. Jo, Y. Kim, J. Moon, S. Park, J. S. Moon, W. B. Park, J. S. Lee and B. H. Hong, *Phys. Chem. Chem. Phys.*, 2015, **17**, 29492–29495.
20 I. Jeon, R. Sakai, S. Seo, G. E. Morse, H. Ueno, T. Nakagawa, Y. Qian, S. Maruyama and Y. Matsuo, *J. Mater. Chem. A*, 2018, **6**, 5746-5751 .
21 S. Berny, N. Blouin, A. Distler, H.-J. Egelhaaf, M. Krompiec, A. Lohr, O. R. Lozman, G. E. Morse, L. Nanson, A. Pron, T. Sauermann, N. Seidler, S. Tierney, P. Tiwana, M. Wagner and H. Wilson, *Adv. Sci.*, 2016, **3**, 1500342.
22 T. W. Shanley, A. A. Martin, I. Aharonovich and M. Toth, *Appl. Phys. Lett.*, 2014, **105**, 063103.
23 A. M. Rao, P. C. Eklund, S. Bandow, A. Thess and R. E. Smalley, *Nature*, 1997, **388**, 257–259.
24 A. Das, S. Pisana, B. Chakraborty, S. Piscanec, S. K. Saha, U. V. Waghmare, K. S. Novoselov, H. R. Krishnamurthy, A. K. Geim, A. C. Ferrari and A. K. Sood, *Nat. Nanotechnol.*, 2008, **3**, 210–215.
25 M. A. Bissett, S. Konabe, S. Okada, M. Tsuji, and H. Ago, *ACS Nano*, 2013, **7**, 10335–10343.
26 R. D. Howells and J. D. Mc Cown, *Chem. Rev.*, 1977, **77**, 69–92.
27 S. Tongay, K. Berke, M. Lemaitre, Z. Nasrollahi, D. B. Tanner, A. F. Hebard and B. R. Appleton, *Nanotechnology*, 2011, **22**, 425701.
28 H. Park, P. R. Brown, V. Bulović and J. Kong, *Nano Lett.*, 2012, **12**, 133–140.
29 Y.-L. Liu, Y.-H. Su, C.-M. Chang, Suryani, D.-M. Wang and J.-Y. Lai, *J. Mater. Chem.*, 2010, **20**, 4409.
30 J. Wang, M. Musameh and Y. Lin, *J. Am. Chem. Soc.*, 2003, **125**, 2408–2409.
31 K. Lee, J.-W. Lee, S.-I. Kim and B. Ju, *Carbon*, 2011, **49**, 787–792.

32 B. J. Landi, R. P. Raffaelle, M. J. Heben, J. L. Alleman, W. VanDerveer and T. Gennett, *Nano Lett.*, 2002, **2**, 1329–1332.
33 T. Takenobu, T. Takano, M. Shiraishi, Y. Murakami, M.Ata, H. Kataura, Y. Achiba and Y. Iwasa, *Nat. Mater.*, 2003, **2**, 683–688.
34 G. U. Sumanasekera, J. L. Allen, S. L. Fang, A. L. Loper, A. M. Rao and P. C. Eklund, *J. Phys. Chem. B*, 1999, **103**, 4292–4297.
35 H. Sung, N. Ahn, M. S. Jang, J.-K. Lee, H. Yoon, N. G. Park and M. Choi, *Adv. Energy Mater.*, 2016, **6**, 1501873
36 J. Yoon, H. Sung, G. Lee, W. Cho, N. Ahn, H. S. Jung and M. Choi, *Energy Environ. Sci.*, 2017, **10**, 337–345.
37 B. Dong, L. Gwee, D. Salas-de la Cruz, K. I. Winey and Y. A. Elabd, *Nano Lett.*, 2010, **10**, 3785–3790.
38 H.-Z. Geng, K. K. Kim, C. Song, N. T. Xuyen, S. M. Kim, K. A. Park, D. S. Lee, K. H. An, Y. S. Lee, Y. Chang, Y. J. Lee, J. Y. Choi, A. Benayad and Y. H. Lee, *J. Mater. Chem.*, 2008, **18**, 1261-1266.
39 I. Jeon, R. Sakai, T. Nakagawa, H. Setoguchi and Y. Matsuo, *Org. Electron.*, 2016, **35**, 193–198.
40 G. Li, R. Zhu and Y. Yang, *Nat. Photonics*, 2012, **6**, 153–161.
41 T.-H. Han, H. Kim, S.-J. Kwon and T.-W. Lee, *Mater. Sci. Eng. R Rep.*, 2017, **118**, 1–43.